ACS OMEGA

Open Access

http://pubs.acs.org/journal/acsodf

Article

Open Thermal Control System for Stable Polymerase Chain Reaction on a Digital Microfluidic Chip

Jiajian Ji, Chenxuan Hu, Xinpei Pang, Jiancong Liang, Qi Huang, Siyi Hu, Qian Mei,* and Hanbin Ma*

Cite This: *ACS Omega* 2024, 9, 10937−10944

Read Online

ACCESS | Metrics & More | Article Recommendations | Supporting Information

ABSTRACT: In this paper, a digital microfluidic thermal control system was introduced for the stable polymerase chain reaction (PCR). The system consists of a thermoelectric cooler unit, a thermal control board, and graphical-user-interface software capable of simultaneously achieving temperature control and on-chip droplet observation. A fuzzy proportional-integral-derivative (PID) method was developed for this system. The simulation analysis was performed to evaluate the temperature of different reagents within the chip. Based on the results, applying fuzzy PID control for PCR will enhance the thermal stability by 67.8% and save the time by 1195 s, demonstrating excellent dynamic response capability and thermal robustness. The experimental results are consistent with the simulation results on the planar temperature distribution, with a data consistency rate of over 99%. The PCR validation was carried out on this system, successfully amplifying the rat GAPDH gene at a concentration of 193 copies/μL. This work has the potential to be useful in numerous existing lab-on-a-chip applications.

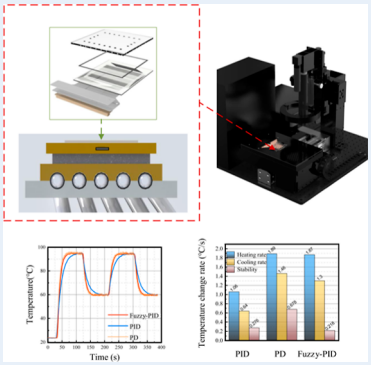

1. INTRODUCTION

The polymerase chain reaction (PCR) technology, which enables in vitro amplification of target nucleic acid sequences,[1,2] is widely recognized as the gold standard in the molecular biology technique due to its sensitivity and accuracy.[3] Compared to bulky and expensive PCR thermal cyclers,[4,5] the point-of-care testing (POCT) devices based on the microfluidic chip technology (also known as lab-on-a-chip) have garnered significant attention.[6−8] These devices offer advantages such as reduced reagent volume, rapid reaction time, easy-to-use, and portability.

In many lab-on-a-chip techniques, electrowetting-on-dielectric (EWOD) digital microfluidics (DMF) enables an independent manipulation of discrete droplets in a reconfigurable and programmable manner, precluding the need for propulsion devices such as pumps and valves.[9] Furthermore, a DMF core unit can be easily integrated and packaged into a fully automated system.[10] This eliminates the need for manual operations, reduces the risk of contamination in multistep nucleic acid analysis, and makes DMF an ideal platform for POC settings.[11−13]

Commercial PCR thermal cyclers typically adopt a closed design to minimize external interference, as shown in Figure 1a. In the application of microfluidic chips, some studies have adopted the structure depicted in Figure 1b. The heating films or heating wires were used as the heat source, and therefore can only be used in isothermal amplification.[14−16] However, an open design, as shown in Figure 1c, is needed for the DMF chip, due to the need for on-chip real-time droplet observation and sample detection.[17,18] In 2008, Pamula et al. first achieved PCR amplification on the DMF chip, using two heating bars to

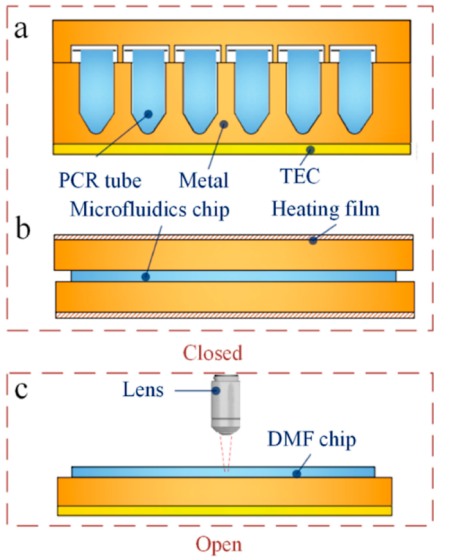

Figure 1. Scheme of (a) commercial PCR thermal cyclers; (b) isothermal amplification for microfluidics chip; and (c) PCR amplification for the DMF chip.

Received: December 23, 2023
Revised: January 31, 2024
Accepted: February 7, 2024
Published: February 19, 2024

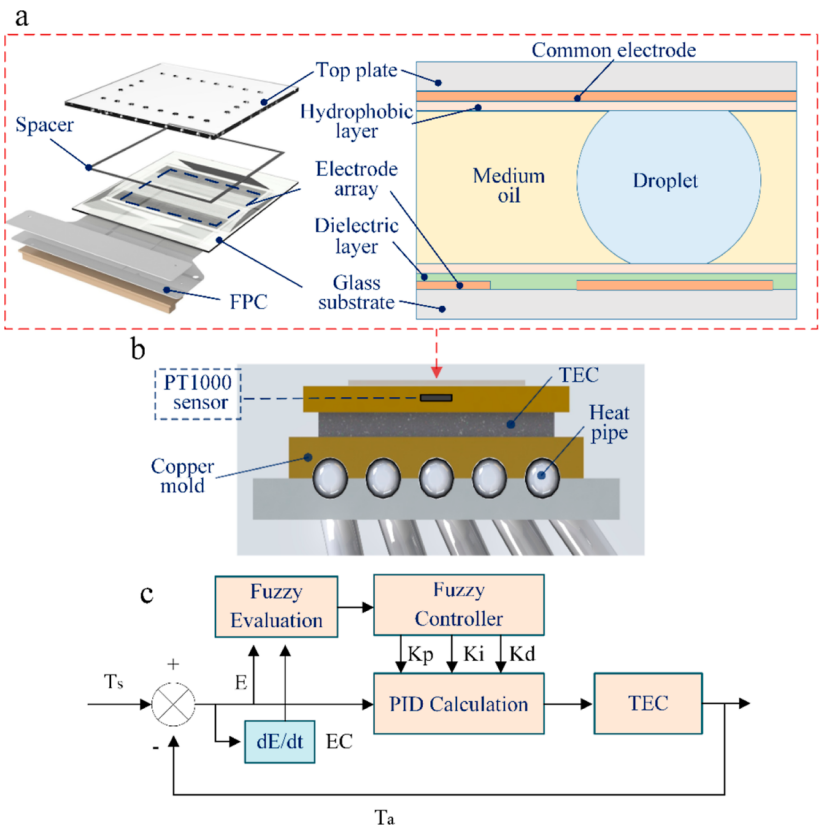

Figure 2. (a) Scheme and cross-section view of the DMF chip; (b) TEC unit structure diagram; and (c) fuzzy PID algorithm principle.

heat specific areas of the chip.[19] Yao and Lin introduced EWOD systems for DNA reaction and analysis, three microheaters with three independent temperature zones.[20] In 2014, Norian et al. integrated a thermal resistor and a thermal sensor with the EWOD electrode, and the chip was mounted using a ball-grid-array package.[21] These studies all involve heating specific areas of the chip for PCR amplification.

However, with the development of the digital microfluidic technology, the number of electrodes has been further increased to achieve higher parallel processing capabilities. In our previous work, the number of electrodes in a chip was 4096, with a single droplet volume of 10 nL.[22,23] Existing temperature control methods cannot meet the requirements of high-throughput DMF chips, especially for scenarios such as droplet digital PCR and single-cell genomics that require temperature control for a large number of droplets.[24,25] These scenarios require the consideration of the planar and vertical temperature distribution inside the chip, which has not been previously studied. Therefore, in DMF technology, an open thermal control system that ensures precise temperature control over a wide range is desirable.

In this paper, an open thermal control system was introduced for stable PCR within a DMF chip. The heating unit using a thermoelectric cooler (TEC) along with its control circuitry and graphical-user-interface (GUI) software for a computer was developed. A fuzzy PID control method was proposed to improve the temperature control performance. In the experiment, k-type thermocouples and a thermal imaging camera were used to obtain the temperature distribution on a chip. Simulation analysis was performed by using COMSOL Multiphysics to evaluate the temperature of different reagents within the chip. Finally, the gene fragment containing rat GAPDH was successfully amplified on the proposed temperature control system, which is expected to have broad applications in the POCT field.

2. MATERIALS AND METHODS

2.1. DMF Chip Fabrication. The scheme of the DMF chip is shown in Figure 2a, which consists of a top plate, a spacer, a glass substrate, and a flexible printed circuit (FPC). The top plate contained holes for injecting liquid samples using pipettes, while indium tin oxide was deposited underneath the top plate as a common electrode. A 100 μm thick spacer was cut from double-sided tape (3M-300LSE, USA) and placed between the top plate and the glass substrate to form a gap. The silicone oil was used as a medium oil to fill the gap for droplet movement. The electrode array was fabricated on the glass substrate through mask electronic manufacturing, and a 300 nm dielectric layer was deposited on the array, as shown in Figure 2a. The electrodes were coated with polytetrafluoroethylene as a hydrophobic layer using a spin coater (WS-650−23NPPB, Laurell). An FPC was connected to the DMF chip for interfacing with a customized chip driving board. These above-mentioned components were designed and assembled by ACXEL Micro & Nano Tech (Foshan, China).

When a voltage was applied to the substrate electrode and common electrode, the solid−liquid interfacial tension decreased, reducing the contact angle from θ_0 to θ_v. The relationship between the forces acting on droplets and the applied voltage can be described by Young's equation and the Young−Lippman equation. The above two equations constitute the fundamental equations for digital microfluidic droplet manipulation; more details can be found in Supporting Information 1.

https://doi.org/10.1021/acsomega.3c10312
ACS Omega 2024, 9, 10937−10944

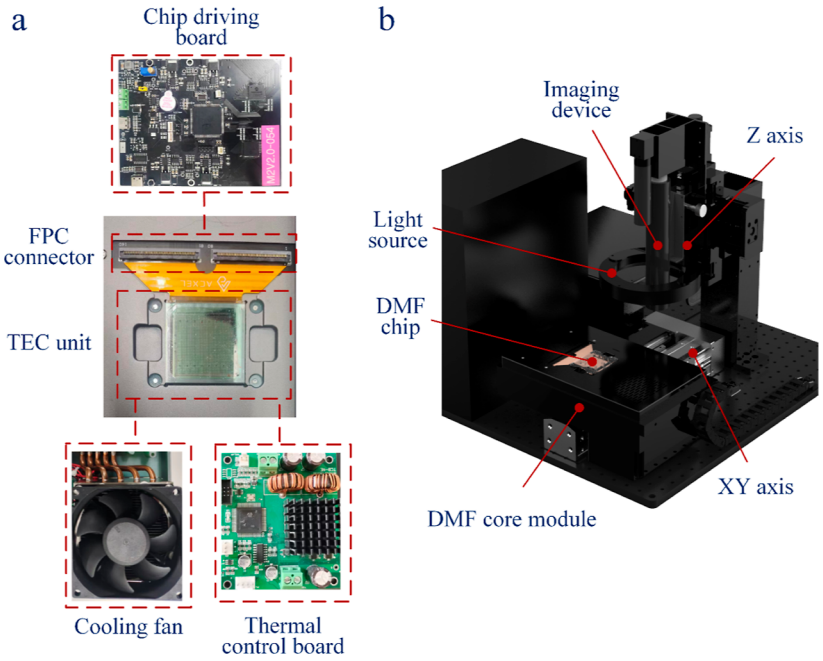

Figure 3. (a) Schematic diagram of the DMF core module and (b) integrated DMF control, movement, and imaging platform.

2.2. Thermal Control Module. This research designed a TEC unit, utilizing a 240 W and 65 mm × 65 mm × 6 mm TEC plate (Haida Tech, China), as depicted in Figure 2b. A 1.5 mm custom copper mold was designed and manufactured using computer-aided design software and computer numerical control machine, and then it was installed on the top and bottom surfaces of the TEC. The contact surfaces between copper and TEC were filled with thermally conductive silicone grease. The top surface was used for placing the DMF chip, and the bottom surface was connected to a cooling fan by a heat pipe.

In order to achieve a precise temperature, a PID feedback control circuit was developed. The circuit block diagram and principle of the PID algorithm are provided in Figure S1 and Supporting Information 2. The PT1000 temperature sensor was inserted into the mounting slot of the copper mold to obtain the temperature. The A/D converter (ADS131-M08IPBS, TI) transformed the temperature signal into a digital signal, and the PID calculation was performed with a microcontroller (MCU, STM32F405, ST). The calculation result was a pulse width modulation (PWM) signal, which was outputted to the gate of a metal-oxide-semiconductor field-effect transistor (MOSFET, DRV8432DKD, ST), and the MOSFET amplified the PWM signal and outputted it to TEC. Tab. S1 lists the electronic component models and manufacturers required for the PID control circuit. These components were all soldered onto a thermal control board. We also conducted noise analysis on the designed circuit, as detailed in Supporting Information 4.

A parameter-adaptive fuzzy PID control algorithm was proposed to enhance the dynamic response performance and stability of the system. The principle of the fuzzy PID algorithm is illustrated in Figure 2c, where T_s is the target temperature, and T_a is the actual temperature of TEC. In the fuzzy PID controller, the E represents the temperature error ($E = T_s - T_a$) and its domain is (−2, 75) according to the experimental test; the EC represents the change rate of error (EC = dE/dt) and its domain is (−0.2, 2); the values of E and EC are taken as NS, O, PS, PM, and PB, corresponding to negative small, zero, positive small, positive middle, and positive big; ΔK_p is the adjustment amount of the proportional coefficient and its domain is (−0.5, 0.5); ΔK_i is the adjustment amount of the integral coefficient and its domain is (−0.006, 0.006); and ΔK_d is the adjustment amount of the derivative coefficient and its domain is (−2, 2). The variables E and EC will be calculated according to the measured value from PT1000, and then the PID parameters (K_p, K_i, K_d) will be adjusted based on the fuzzy controller. The more details about the designed fuzzy controller in this article can be found in Supporting Information 3. The entire process is dynamically adjusted in real-time. The fuzzy PID algorithm was uploaded to the MCU after being compiled by Keil 5 IDE software.

GUI software based on the C# programming language was developed to enable the communication between the computer and the thermal control board, as shown in Figure S2.

2.3. Integrated DMF Platform Setup. Figure 3a indicates the schematic diagram of the DMF core module. The driving signals generated by the chip driver board (developed by ACXEL Micro & Nano Tech) were outputted to the electrode array via an FPC connector. The cooling fan provided heat conduction for the TEC unit, while the thermal control board performed PID adjustment on the TEC (see Section 2.2 for more details). A 3D-printed housing had been designed and fabricated for the installation of the DMF core module, as shown in Figure S3.

The DMF platform, illustrated in Figure 3b, comprises the chip, a core module, *XY* and *Z* movement axes, and GUI software, as well as an imaging device and light source. The high-speed camera (Hikvision, China), combined with a lens, formed an imaging device used for image acquisition. The XY axis was used for the field of view movement, while the *Z* axis adjusted the focal distance. The GUI software integrated functions such as the image display of droplet positions, generation of droplet motion paths, and path execution.

https://doi.org/10.1021/acsomega.3c10312
ACS Omega 2024, 9, 10937−10944

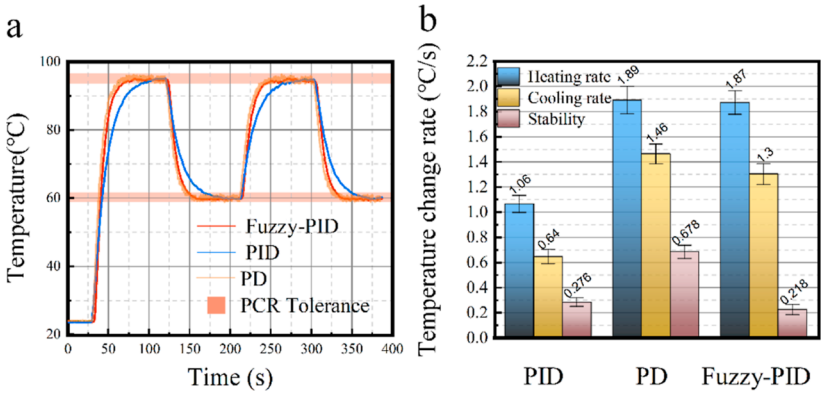

Figure 4. (a) Temperature curves using different algorithms and (b) comparison of performance indicators.

2.4. Temperature Control Performance Test. As the most commonly used temperatures for PCR, 95 °C (denaturation) and 60 °C (annealing)[26] were chosen as the target test temperatures for this experiment. Compared to PT1000 sensors, thermocouples may have a lower measurement range and accuracy at low temperatures. However, their smaller size makes them more suitable for temperature measurements on flat surfaces. Figure S4 illustrates the temperature control performance experiment, where a K-type surface-mount thermocouple (Kaipusen, China) was employed to measure the temperatures of the DMF chip's top plate and glass substrate. The temperature data were uploaded to a PC using a USB-2400 multifunction data acquisition device (OMEGA, USA). The target temperature was set in thermal GUI, and the results of temperature variation over time were automatically recorded on the PC. In addition, a thermal imaging camera (FOTRIC, China) was used to capture the temperature distribution on the surface of the chip.

2.5. Simulation Analysis Settings. The internal temperature of the chip was simulated and analyzed by using the COMSOL Multiphysics software. The three-dimensional simulation was performed using the Solid and Fluid Heat Transfer module in COMSOL. The intermediate layer materials were set as air, water (the main components of the PCR mixture), and silicone oil (medium oil), respectively. For the boundary conditions, the temperature of the glass substrate was set to 60 and 95 °C, and the heat dissipation condition was defined as surface-to-environment radiation during an ambient temperature of 26 °C. The meshing was carried out using the physics-controlled meshing, resulting in the mesh shown in Figure S5.

2.6. Reagents. Deionized water (purified from a Milli-Q water purification system) and isopropyl alcohol (purchased from Sinopharm Chemical Reagent) were mainly used for washing the chip. Silicone oil and the surfactant Pluronic F68 were purchased from Sigma-Aldrich. 2× PowerUp SYBR Green Master Mix and UltraPure DNase/RNase-Free Distilled water were purchased from Thermo Fisher Scientific. The 193 copies/μL of genomic DNA (gDNA) was extracted from CHO cells (purchased from the Cell Resource Center of CAS) using a magnetic bead nucleic acid extraction kit (purchased from Vazyme Biotech Co., Ltd.). A pair of forward and reverse primers, as listed in Table S2, were designed to detect the rat GAPDH gene fragment in the gDNA.

2.7. PCR Assay. The 50 μL positive PCR mixture was premixed outside the chip, including 25 μL of 2× SYBR Green master mix, 4 μL of 1% F68, 14 μL of DNase/RNase-Free water, 1 μL of each forward and reverse primers (10 μM), and 5 μL of template DNA. For the negative mixture, the same reagent components as the positive mixture were used, except that the template DNA was replaced with 5 μL of DNase/RNase-Free water. Finally, the concentration of the template DNA was 193 copies/μL in a positive PCR mixture after mixing. The positive and negative PCR mixtures were injected into the chip from two different injection ports using a pipette. By using a predetermined moving path as shown in Movie S1, the PCR mixtures were partitioned into 0.1 μL droplets within the chip and moved to their designated positions. The PCR cycling temperature and time were set in the thermal GUI software according to Table S3, followed by initiation of the temperature control program. After the completion of PCR, the chip was transferred to a Nikon ECLIPSE Ni−U microscope for fluorescence observation.

3. RESULTS AND DISCUSSION

3.1. Different Algorithm Evaluation. Figure 4 indicates the PCR temperature curves by using different algorithms. In this section, the performance of PID, PD (removing the integral term), and the proposed fuzzy PID was compared by defining three evaluation metrics for temperature: heating rate, cooling rate, and stability (calculated from the standard deviation at 95 °C). The obtained curve using the PD algorithm has the fastest heating/cooling rates, which are 1.89 and 1.46 °C/s, respectively. However, it exhibits poor temperature control robustness, and the standard deviation is 0.678 °C, which may affect the PCR cycling. The PID curve exhibits a heating rate of 1.06 °C/s and cooling rate of 0.64 °C/s.

On the contrary, the fuzzy PID demonstrates good response performance while maintaining excellent robustness. Its heating and cooling rates are 1.87 and 1.3 °C/s, which is similar to PD, as shown in Figure 4b. However, the stability has significantly improved by 67.8%. In addition, under the same hardware conditions, using the fuzzy PID for PCR (assuming 40 cycles) would save the reaction time of 1195 s compared to PID.

3.2. Temperature Profile and Simulation Result. Due to the small size of the chip, existing methods cannot directly measure the internal temperature of the chip. Herein, the temperature profiles of the chip's top plate and substrate were obtained using K-type thermocouples. The temperatures of different reagents inside the chip were obtained through finite element analysis with the COMSOL Multiphysics software. The results were exported from the software and plotted. The

https://doi.org/10.1021/acsomega.3c10312
ACS Omega 2024, 9, 10937−10944

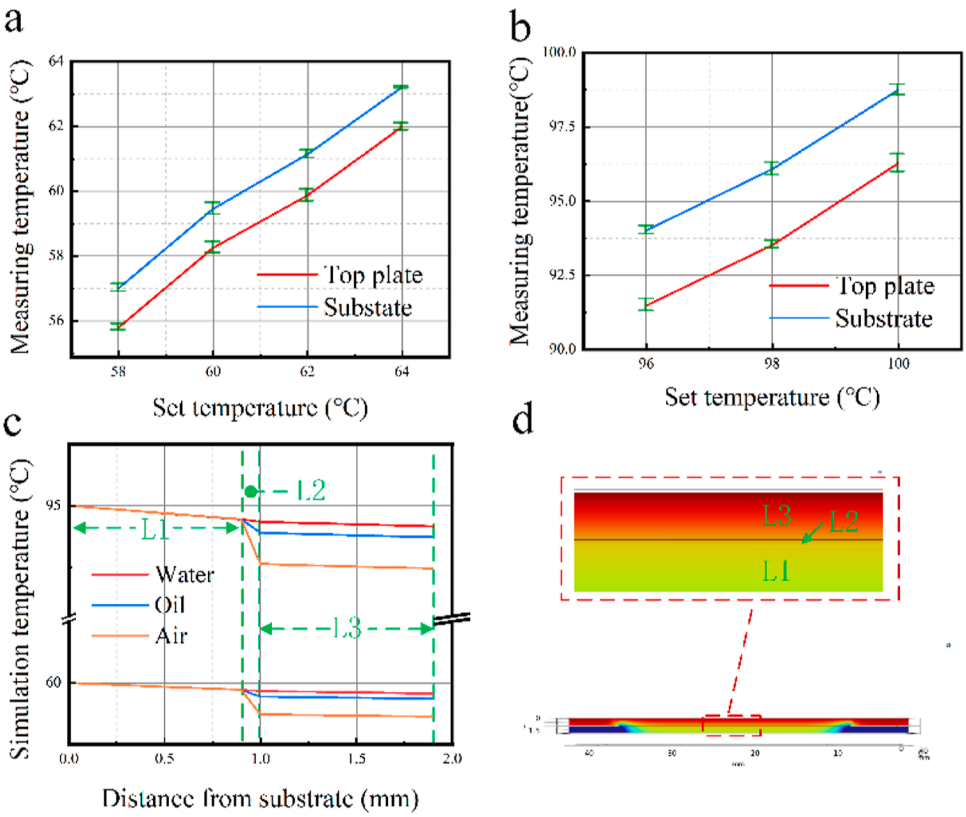

Figure 5. (a) Measuring temperature profiles at the annealed/extended stage; (b) measuring temperature profiles at the denatured stage; (c) simulation temperature profiles; and (d) temperature cross-section diagram of simulation analysis.

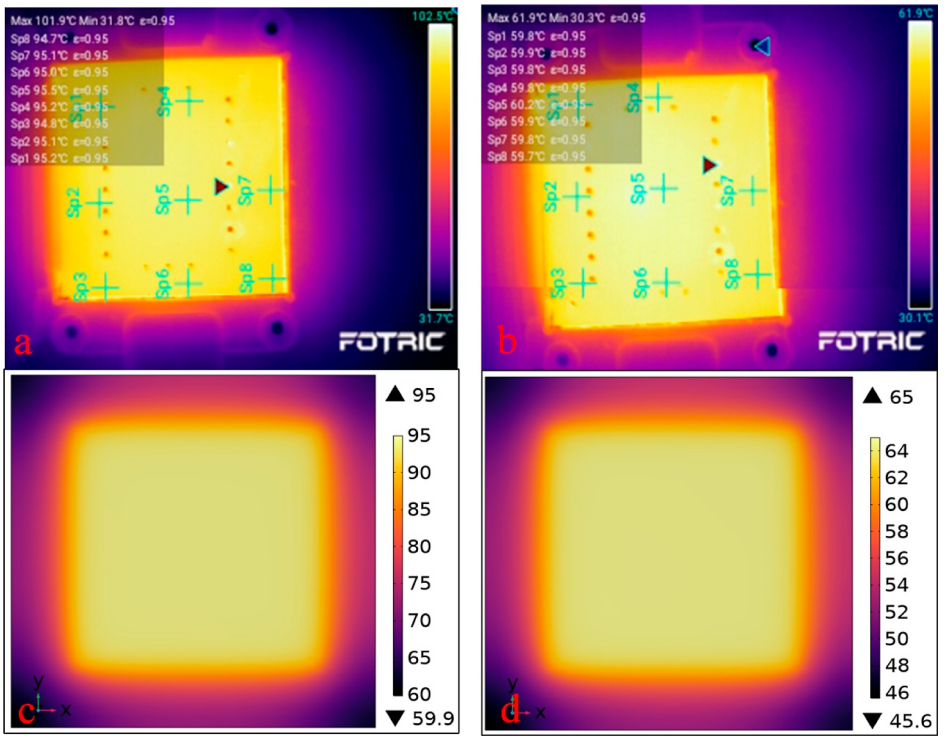

Figure 6. Temperature distribution on the chip. (a) Thermal imaging result at 95 °C; (b) thermal imaging result at 60 °C; (c) simulation result at 95°C; and (d) simulation result at 60 °C.

x-axis is the distance from the bottom surface of the chip in Figure 5c,d, where L1 represents the glass substrate layer (0.9 mm), L2 represents the intermediate layer (0.1 mm), and L3 represents the top plate (0.9 mm).

https://doi.org/10.1021/acsomega.3c10312
ACS Omega 2024, 9, 10937−10944

The temperature difference between the set temperature and the chip substrate is 0.8 °C in Figure 5a, and the temperature difference is 1.3°C in Figure 5b. When the medium is air, the temperature differences between the top plate and substrate are 1.22 °C in Figure 5a and 2.50 °C in Figure 5b. From the simulation results, the temperature difference (orange curve) is 1.32 and 2.56 °C, respectively. This indicates that the simulation model is capable of accurately simulating trials and providing valuable predictions and analysis. In addition, the temperature of water within the chip is 94.4 ± 0.05 °C and 59.75 ± 0.03 °C.

The thermal imaging and simulated planar temperature distribution are shown in Figure 6. The results of comparing 8 selected points in the images are listed in Table S4. The simulation results are consistent with the experimental results with a data consistency rate of over 99%. In Figure 6a,b, the average values with standard deviation are 95.07 ± 0.23 °C and 59.86 ± 0.14 °C, respectively; while the values in Figure 6c,d are 95.11 ± 0.07 °C and 59.97 ± 0.035 °C. According to the infrared imaging results, the thermal uniformity of the DMF chip at 95 and 60 °C is 0.233 and 0.140 °C, respectively.

3.3. PCR Assay. In order to verify the system, an experiment was conducted using a PCR reagent kit; the experimental steps have been introduced in Section 2.7. The 5 × 5 microdroplets with a volume of 0.1 μL per droplet are distributed within the DMF chip, as shown in Figure 7a. The

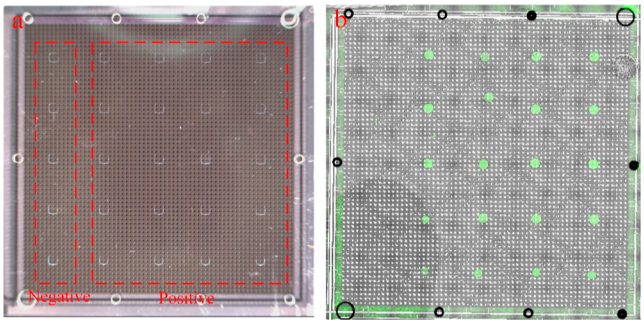

Figure 7. (a) Negative and positive droplets before PCR and (b) fluorescence signal detection results after PCR.

leftmost 5 droplets are negative controls without the addition of template DNA, while the remaining 20 droplets are positive groups containing the rat GAPDH gene. Figure 7b shows the fluorescence detection results by using an FITC channel. All positive droplets showed detectable fluorescence signals, indicating that the proposed system meets the requirements for PCR.

3.4. Discussion. Table 1 provides a comparison between the parameters of existing microfluidic temperature control systems and those of the current study, highlighting the exceptional performance of this system in terms of temperature range and temperature control accuracy.

4. CONCLUSIONS

This paper describes an open thermal control system composed of a TEC unit, heat control board, and GUI software. The control strategies of TEC to achieve temperature control on the DMF chip are further analyzed through simulation and experiments. The following results were obtained:

1 A fuzzy PID algorithm was proposed, which enhanced the system stability by 67.8% and saved the time by 1195 s during a PCR process.
2 Through simulation and experiments, the linear relationship between the chip temperature and the set temperature was analyzed. The actual temperatures of the reagents inside the chip were found to be 94.4 ± 0.05 °C and 59.75 ± 0.03 °C.
3 The thermal uniformity for the planar temperature distribution was 0.233 °C at 95 °C and 0.140 °C at 60 °C, respectively.
4 The biomedical application of the system was validated, and a gene fragment with a concentration of 193 copies/μL was successfully amplified.

Based on the above results, an open thermal control system was developed for PCR amplification, which shows the exceptional performance of this system in terms of temperature range and temperature control accuracy. This system is capable of simultaneously achieving temperature control and on-chip droplet observation, which enables improved application of lab-on-a-chip technology for the POCT field.

■ ASSOCIATED CONTENT

Data Availability Statement

Data will be made available on request.

Supporting Information

The Supporting Information is available free of charge at https://pubs.acs.org/doi/10.1021/acsomega.3c10312.

Video of sample injection, droplet of generation and movement (MP4)

Fundamental equations for digital microfluidic droplet manipulation, principle of the PID algorithm, designed fuzzy controller, noise analysis on the designed circuit, PID feedback control block diagram, GUI for communication with the thermal control board, DMF core module in a 3D-printed housing, temperature control performance experiment, meshing result, com-

Table 1. Comparison between the Previous and Current Work

study	temperature range (°C)	stability(°C)	uniformity(°C)	description
27	26 to 90+	3.05	uncertain	closed system for PCR
28	−25 to 10	0.309	uncertain	constant temperature control
29	2 to 37	0.3	0.24	constant temperature control
30	−35 to 0	0.4	uncertain	constant temperature control
15	26 to 35	uncertain	0.4	constant temperature control
31	26 to 37	0.1	uncertain	constant temperature control
32	26 to 95	1	uncertain	open system for PCR
this work	26 to 95	0.218	0.233 °C at 95 °C, 0.14 °C at 60 °C	open system for PCR

https://doi.org/10.1021/acsomega.3c10312
ACS Omega 2024, 9, 10937−10944

ponent list for the PID control circuit, primer sequence for the DNA template, PCR standard cycling mode, comparison of 8 points between thermal imaging and simulation, and Video of sample injection, droplet of generation and movement (PDF)

AUTHOR INFORMATION

Corresponding Authors

Qian Mei − *School of Biomedical Engineering (Suzhou), Division of Life Sciences and Medicine, University of Science and Technology of China, Hefei 230026, China; CAS Key Laboratory of Biomedical Diagnostics, Suzhou Institute of Biomedical Engineering and Technology, Chinese Academy of Sciences (CAS), Suzhou 215163, China*; Email: qmei@sibet.ac.cn

Hanbin Ma − *School of Biomedical Engineering (Suzhou), Division of Life Sciences and Medicine, University of Science and Technology of China, Hefei 230026, China; CAS Key Laboratory of Biomedical Diagnostics, Suzhou Institute of Biomedical Engineering and Technology, Chinese Academy of Sciences (CAS), Suzhou 215163, China;* orcid.org/0000-0002-7629-2287; Email: mahb@sibet.ac.cn

Authors

Jiajian Ji − *School of Biomedical Engineering (Suzhou), Division of Life Sciences and Medicine, University of Science and Technology of China, Hefei 230026, China; CAS Key Laboratory of Biomedical Diagnostics, Suzhou Institute of Biomedical Engineering and Technology, Chinese Academy of Sciences (CAS), Suzhou 215163, China;* orcid.org/0000-0002-4058-2733

Chenxuan Hu − *School of Biomedical Engineering (Suzhou), Division of Life Sciences and Medicine, University of Science and Technology of China, Hefei 230026, China; CAS Key Laboratory of Biomedical Diagnostics, Suzhou Institute of Biomedical Engineering and Technology, Chinese Academy of Sciences (CAS), Suzhou 215163, China*

Xinpei Pang − *School of Biomedical Engineering (Suzhou), Division of Life Sciences and Medicine, University of Science and Technology of China, Hefei 230026, China; CAS Key Laboratory of Biomedical Diagnostics, Suzhou Institute of Biomedical Engineering and Technology, Chinese Academy of Sciences (CAS), Suzhou 215163, China*

Jiancong Liang − *Guangdong ACXEL Micro & Nano Tech Co., Ltd, Foshan 528200, China*

Qi Huang − *CAS Key Laboratory of Biomedical Diagnostics, Suzhou Institute of Biomedical Engineering and Technology, Chinese Academy of Sciences (CAS), Suzhou 215163, China;* orcid.org/0000-0002-7370-2113

Siyi Hu − *CAS Key Laboratory of Biomedical Diagnostics, Suzhou Institute of Biomedical Engineering and Technology, Chinese Academy of Sciences (CAS), Suzhou 215163, China;* orcid.org/0000-0002-0686-5182

Complete contact information is available at: https://pubs.acs.org/10.1021/acsomega.3c10312

Funding

This research was funded by the National Key R&D Program of China (no. 2023YFC2412900), the National Natural Science Foundation of China (nos. 82172077, 22201298, 62374102, and 62027825), the Innovation and Entrepreneurship Team of Jiangsu Province (JSSCTD202145), and the Science and Technology Development Project of Jilin Province (20210204110YY).

Notes

The authors declare no competing financial interest.

REFERENCES

(1) Mullis, K. B.; Faloona, F. A.; Scharf, S. J.; Saiki, R. K.; Horn, G.; Erlich, H. Specific Enzymatic Amplification of DNA In Vitro: The Polymerase Chain Reaction. *Cold Spring Harbor Symp. Quant. Biol.* **1986**, *51*, 263−273.

(2) Avni, T.; Leibovici, L.; Paul, M. PCR Diagnosis of Invasive Candidiasis: Systematic Review and Meta-Analysis. *J. Clin. Microbiol.* **2011**, *49*, 665−670.

(3) Kovarik, M. L.; Ornoff, D. M.; Melvin, A. T.; Dobes, N. C.; Wang, Y.; Dickinson, A. J.; Gach, P. C.; Shah, P. K.; Allbritton, N. L. Micro total analysis systems: fundamental advances and applications in the laboratory, clinic, and field. *Anal. Chem.* **2013**, *85*, 451−472.

(4) Nguyen, H. V.; Phan, V. M.; Seo, T. S. Total integrated centrifugal genetic analyzer for point-of-care Covid-19 testing with automatic and high-throughput capability. *Sens. Actuators, B* **2022**, *353*, 131088.

(5) Wang, C.; Liu, M.; Wang, Z.; Li, S.; Deng, Y.; He, N. Point-of-care diagnostics for infectious diseases: From methods to devices. *Nano Today* **2021**, *37*, 101092.

(6) Nguyen, V. D.; Van Nguyen, H.; Seo, J. W.; Lee, S. H.; Seo, T. S. Prediction of acute rejection in kidney transplanted patients based on the point-of-care isothermal molecular diagnostics platform. *Biosens. Bioelectron.* **2022**, *199*, 113877.

(7) Nguyen, H. V.; Nguyen, V. D.; Lee, E. Y.; Seo, T. S. Point-of-care genetic analysis for multiplex pathogenic bacteria on a fully integrated centrifugal microdevice with a large-volume sample. *Biosens. Bioelectron.* **2019**, *136*, 132−139.

(8) Xie, M.; Chen, T.; Cai, Z.; Lei, B.; Dong, C. A digital microfluidic platform coupled with colorimetric loop-mediated isothermal amplification for on-site visual diagnosis of multiple diseases. *Lab Chip* **2023**, *23*, 2778−2788.

(9) Schell, W. A.; Benton, J. L.; Smith, P. B.; Poore, M.; Rouse, J. L.; Boles, D. J.; Johnson, M. D.; Alexander, B. D.; Pamula, V. K.; Eckhardt, A. E.; Pollack, M. G.; Benjamin, D. K., Jr.; Perfect, J. R.; Mitchell, T. G. Evaluation of a digital microfluidic real-time PCR platform to detect DNA of Candida albicans in blood. *Eur. J. Clin. Microbiol. Infect. Dis.* **2012**, *31*, 2237−2245.

(10) Zhong, Z.; Li, Z.; Chakrabarty, K.; Ho, T. Y.; Lee, C. Y. Micro-Electrode-Dot-Array Digital Microfluidic Biochips: Technology, Design Automation, and Test Techniques. *IEEE Trans. Biomed. Circuits Syst.* **2019**, *13*, 292−313.

(11) Ma, H.; Shi, S.; Jin, K.; Wang, D.; Hu, S.; Su, Y.; Zhang, Y.; Li, J.; Liu, Z.; Jiang, C.; Feng, L.; Guo, X.; Nathan, A. Large-area manufacturable active matrix digital microfluidics platform for high-throughput biosample handling. 2020 IEEE International Electron Devices Meeting (IEDM), 2020; pp 35.35.31−35.35.34.

(12) Xu, X.; Cai, L.; Liang, S.; Zhang, Q.; Lin, S.; Li, M.; Yang, Q.; Li, C.; Han, Z.; Yang, C. Digital microfluidics for biological analysis and applications. *Lab Chip* **2023**, *23*, 1169−1191.

(13) Xu, Y.; Wu, W.; Zhou, Z.; Su, Q.; Liu, X.; Li, W.; Wang, K. Digital Microfluidic Lab-on-a-Chip on a TFT Glass Substrate Enabling Point-of-Care Testing. *IEEE Electron Device Lett.* **2023**, *44*, 1500−1503.

(14) Nguyen, H. V.; Phan, V. M.; Seo, T. S. A portable centrifugal genetic analyzer for multiplex detection of feline upper respiratory tract disease pathogens. *Biosens. Bioelectron.* **2021**, *193*, 113546.

(15) Shen, J.; Zhang, L.; Yuan, J.; Zhu, Y.; Cheng, H.; Zeng, Y.; Wang, J.; You, X.; Yang, C.; Qu, X.; Chen, H. Digital Microfluidic Thermal Control Chip-Based Multichannel Immunosensor for Noninvasively Detecting Acute Myocardial Infarction. *Anal. Chem.* **2021**, *93*, 15033−15041.

(16) Madadelahi, M.; Madou, M. J. Rational PCR Reactor Design in Microfluidics. *Micromachines* **2023**, *14*, 1533.

(17) Hu, S.; Jie, Y.; Jin, K.; Zhang, Y.; Guo, T.; Huang, Q.; Mei, Q.; Ma, F.; Ma, H. All-in-One Digital Microfluidics System for Molecular Diagnosis with Loop-Mediated Isothermal Amplification. *Biosensors* **2022**, *12*, 324.
(18) Jain, V.; Patrikar, R. M. A Low-Cost Portable Dynamic Droplet Sensing System for Digital Microfluidics Applications. *IEEE Trans. Instrum. Meas.* **2020**, *69*, 3623−3630.
(19) Sista, R.; Hua, Z.; Thwar, P.; Sudarsan, A.; Srinivasan, V.; Eckhardt, A.; Pollack, M.; Pamula, V. Development of a digital microfluidic platform for point of care testing. *Lab Chip* **2008**, *8*, 2091.
(20) Lin, T.-H.; Yao, D.-J. Applications of EWOD Systems for DNA Reaction and Analysis. *J. Adhes. Sci. Technol.* **2012**, *26*, 1789−1804.
(21) Norian, H.; Field, R. M.; Kymissis, I.; Shepard, K. L. An integrated CMOS quantitative-polymerase-chain-reaction lab-on-chip for point-of-care diagnostics. *Lab Chip* **2014**, *14*, 4076−4084.
(22) Wang, D.; Wu, S.; Huang, Q.; Chang, C.; Xu, L.; Jin, K.; Hu, S.; Yu, J.; Ma, H. Active-Matrix Digital Microfluidics Design and Optimization for High-Throughput Droplets Manipulation. *IEEE J. Electron Devices Soc.* **2023**, *11*, 411−415.
(23) Hu, S.; Ye, J.; Shi, S.; Yang, C.; Jin, K.; Hu, C.; Wang, D.; Ma, H. Large-Area Electronics-Enabled High-Resolution Digital Microfluidics for Parallel Single-Cell Manipulation. *Anal. Chem.* **2023**, *95*, 6905−6914.
(24) Yin, K.; Zeng, X.; Liu, W.; Xue, Y.; Li, X.; Wang, W.; Song, Y.; Zhu, Z.; Yang, C. Stable Colloidosomes Formed by Self-Assembly of Colloidal Surfactant for Highly Robust Digital PCR. *Anal. Chem.* **2019**, *91*, 6003−6011.
(25) Postek, W.; Garstecki, P. Droplet Microfluidics for High-Throughput Analysis of Antibiotic Susceptibility in Bacterial Cells and Populations. *Acc. Chem. Res.* **2022**, *55*, 605−615.
(26) Saito, M.; Takahashi, K.; Kiriyama, Y.; Espulgar, W. V.; Aso, H.; Sekiya, T.; Tanaka, Y.; Sawazumi, T.; Furui, S.; Tamiya, E. Centrifugation-Controlled Thermal Convection and Its Application to Rapid Microfluidic Polymerase Chain Reaction Devices. *Anal. Chem.* **2017**, *89*, 12797−12804.
(27) Ling, W.; Zhou, W.; Cui, J.; Shen, Z.; Wei, Q.; Chu, X. Experimental study on the heating/cooling and temperature uniformity performance of the microchannel temperature control device for nucleic acid PCR amplification reaction of COVID-19. *Appl. Therm. Eng.* **2023**, *226*, 120342.
(28) Liu, Z.; Sun, D.; Jiang, B.; Shen, L.; Zhou, P.; Gao, C.; Jin, Z.; Liu, X.; Yang, L.; Tan, S. Continuous gradient temperature control of microfluidic chip based on thermoelectric cooler. *Appl. Therm. Eng.* **2023**, *234*, 121277.
(29) Peng, J.; Fang, C.; Ren, S.; Pan, J.; Jia, Y.; Shu, Z.; Gao, D. Development of a microfluidic device with precise on-chip temperature control by integrated cooling and heating components for single cell-based analysis. *Int. J. Heat Mass Transfer* **2019**, *130*, 660−667.
(30) Tarn, M. D.; Sikora, S. N. F.; Porter, G. C. E.; Wyld, B. V.; Alayof, M.; Reicher, N.; Harrison, A. D.; Rudich, Y.; Shim, J. U.; Murray, B. J. On-chip analysis of atmospheric ice-nucleating particles in continuous flow. *Lab Chip* **2020**, *20*, 2889−2910.
(31) Ren, K.; Xie, Y.; Wang, C.; Yan, J.; Shi, Y.; Guo, J.; Guo, J. Application of the fuzzy proportional integral differential (PID) temperature control algorithm in a liver function test system based on a centrifugal microfluidic device. *Talanta* **2024**, *268*, 125330.
(32) Xue, N.; Yan, W. Glass-Based Continuous-Flow PCR Chip With a Portable Control System for DNA Amplification. *IEEE Sensor. J.* **2012**, *12*, 1914−1918.

https://doi.org/10.1021/acsomega.3c10312
ACS Omega 2024, 9, 10937−10944